geosciences

MDPI

Article

The Medicine Hat Block and the Early Paleoproterozoic Assembly of Western Laurentia

Jennifer N. Gifford [1,*], Shawn J. Malone [2] and Paul A. Mueller [3]

[1] Department of Geology and Geologic Engineering, University of Mississippi, Oxford, MS 38677, USA
[2] Department of Environment, Geology, and Natural Resources, Ball State University, Muncie, IN 47304, USA; sjmalone@bsu.edu
[3] Department of Geological Sciences, University of Florida, Gainesville, FL 32611, USA; pamueller@ufl.edu
* Correspondence: jngiffor@olemiss.edu; Tel.: +1-662-915-2079

Received: 12 June 2020; Accepted: 8 July 2020; Published: 15 July 2020

Abstract: The accretion of the Wyoming, Hearne, and Superior Provinces to form the Archean core of western Laurentia occurred rapidly in the Paleoproterozoic. Missing from Hoffman's (1988) original rapid aggregation model was the Medicine Hat block (MHB). The MHB is a structurally distinct, complex block of Precambrian crystalline crust located between the Archean Wyoming Craton and the Archean Hearne Province and overlain by an extensive Phanerozoic cover. It is distinguished on the basis of geophysical evidence and limited geochemical data from crustal xenoliths and drill core. New U-Pb ages and Lu-Hf data from zircons reveal protolith crystallization ages from 2.50 to 3.28 Ga, magmatism/metamorphism at 1.76 to 1.81 Ga, and εHf_T values from −23.3 to 8.5 in the Archean and Proterozoic rocks of the MHB. These data suggest that the MHB played a pivotal role in the complex assembly of western Laurentia in the Paleoproterozoic as a conjugate or extension to the Montana Metasedimentary Terrane (MMT) of the northwestern Wyoming Province. This MMT–MHB connection likely existed in the Mesoarchean, but it was broken sometime during the earliest Paleoproterozoic with the formation and closure of a small ocean basin. Closure of the ocean led to formation of the Little Belt arc along the southern margin of the MHB beginning at approximately 1.9 Ga. The MHB and MMT re-joined at this time as they amalgamated into the supercontinent Laurentia during the Great Falls orogeny (1.7–1.9 Ga), which formed the Great Falls tectonic zone (GFTZ). The GFTZ developed in the same timeframe as the better-known Trans-Hudson orogen to the east that marks the merger of the Wyoming, Hearne, and Superior Provinces, which along with the MHB, formed the Archean core of western Laurentia.

Keywords: Medicine Hat block; U-Pb geochronology; Lu-Hf geochemistry; zircon

1. Introduction

The Precambrian Medicine Hat Block (MHB) lies south of the Archean Hearne Province (Figure 1), and it was originally defined by structural features in overlying Paleozoic sedimentary rocks [1] and subsequently by potential field and seismic surveys [2,3]. Although its history is poorly constrained due to extensive Phanerozoic sedimentary cover (Figure 1), an Archean age for the MHB was first proposed on the basis of multi-grain U-Pb zircon ages acquired by ID-TIMS (isotope dilution-thermal ionization mass spectrometry) from five samples of drill core recovered from oil and gas exploration wells [4]. U-Pb ages of these samples range from approximately 2.6 to 3.3 Ga [4]. With its long history, the MHB clearly occupied an important position between the Wyoming Craton and the Hearne Province during the formation of the supercontinent Laurentia.

In this paper, we focus on refining the evolution of the northwestern crystalline basement of the MHB and western Canada sedimentary basin and relate that history to that of other terranes that

accreted to Laurentia prior to 1.7 Ga. We report results of 484 new single zircon U-Pb ages obtained by laser ablation multi-collector ICP-MS from drill core and xenoliths previously described and analyzed by Villeneuve et al. [4] and Davis et al. [5] in order to extract the maximum information from these unique samples, including all new in situ Lu-Hf analyses by the same method. The xenoliths are from Eocene minettes of the Sweetgrass Hills area of the Montana alkali province (MAP) located within southern Alberta and northern Montana (Figure 1; [6]). These alkaline volcanic-entrained xenoliths provide a unique opportunity to study the age and history of the enigmatic continental crust of the northwestern MHB (e.g., [5,7]) and the buried southern (Alberta) part of the western Canada sedimentary basin [8–13]. Constraining the relationships of the Medicine Hat block to the adjacent Paleoproterozoic belts (e.g., Great Falls Tectonic Zone (GFTZ), Trans-Hudson orogen (THO), and Vulcan low) is important for understanding the geodynamics of the rapid, Paleoproterozoic assembly of Laurentia proposed by Hoffman [14].

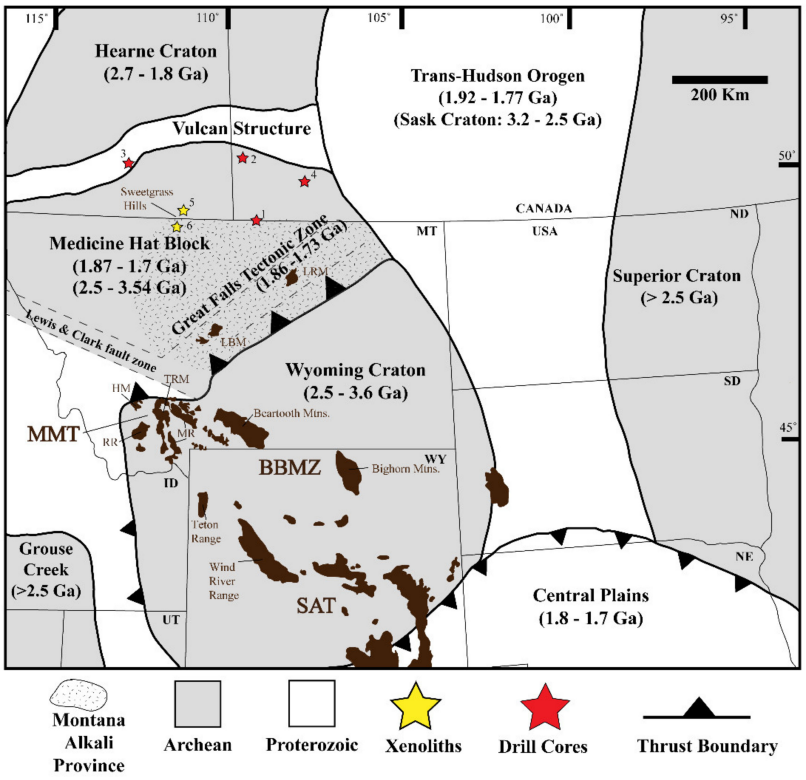

Figure 1. Generalized map of Precambrian basement provinces of southwestern Laurentia with the Montana alkali province (MAP) shown without a solid boundary, as the extent of the MAP is not well known (after [2,15–19]). MMT: Montana Metasedimentary Terrane; BBMZ: Bighorn-Beartooth Magmatic Zone. TRM: Tobacco Root Mountains; HM: Highland Mountains; RR: Ruby Range; MR: Madison Range; LRM: Little Rocky Mountains; LBM: Little Belt Mountains. Drill core locations: (**1**) Home Pacific Knappen; (**2**) Imperial Calstan Lake Newell; (**3**) PCA Calstan Parkland; (**4**) PCP Medicine Hat. Xenolith localities: (**5**) Coulee 29; (**6**) Sill 39.

Geologic Background and Previous Work

The boundary separating the MHB and the Hearne Province to the north is the Vulcan structure, which is a prominent, linear feature characterized by both gravity and magnetic lows (Figure 1; [9]). The northern limit of the MHB in southern Alberta and northern Montana, including the Vulcan structure, is entirely buried beneath the sediments filling the Western Canada sedimentary basin, which is a Cordilleran foreland basin. On its eastern margin, the MHB is bounded by Paleoproterozoic rocks of the Trans-Hudson orogen (Figure 1; [20–22]). To the south, at least parts of the MHB lie within the Great Falls tectonic zone (GFTZ) that formed during the Great Falls orogeny (1.7–1.9 Ga; [23]).

The GFTZ also marks the northern limit of the Archean Beartooth-Bighorn magmatic zone of the Wyoming Province [24,25]. Proposals for the origin of the GFTZ have ranged from Archean and Paleoproterozoic suture zones to an intra-continental shear zone [2,26–28].

South and west of the MHB, the Montana Metasedimentary terrane (MMT; Figure 1) of the Wyoming Province is dominated by >3.0 Ga quartzofeldspathic gneisses in which belts of distinct Archean metasupracrustal rocks are preserved [29–34]. Exposures in the MMT are predominantly in Laramide uplifts, e.g., the Tobacco Root Mountains, Highland Mountains, Madison Range, and Ruby Range [24,25,30–55]. The ages reported from the MMT include: (1) rare Eoarchean ca. 3.93 Ga detrital zircons from Archean quartzites [33,40]; (2) Paleoarchean tonalitic to tronhjemitic gneisses (ca. 3.3 Ga) [32,37]; (3) Neoarchean quartzofeldspathic gneisses and amphibolite-grade metamorphism at ca. 2.7 Ga to 2.8 Ga [31–34,37,41–46]; and (4) Paleoproterozoic metamorphism at 2.45 and 1.7–1.9 Ga [24,30,37–39,45,47–55]. Throughout the MMT, ages representing prograde, peak, and retrograde intervals of metamorphism have been reported from zircon, monazite, micas, and amphibole in the U-Pb, Sm-Nd, and K-Ar systems. This clearly defined approximately 1.7–1.9 Ga event [24,30,37,39,45,47–55] is broadly recorded across western Laurentia, particularly in the K-Ar ($^{40}Ar/^{39}Ar$) system. In addition to the MMT, terranes bordering the MHB and recording this interval of dominantly metamorphic cooling ages include the Vulcan aeromagnetic low [9], GFTZ [28,56–59], and THO [60–67]. The broad geographic range of this event(s) leads to the conclusion that these parts of western Laurentia were fully assembled prior to approximately 1.7 Ga and one or more widespread thermal event(s) likely affected the amalgamated terranes in the interval from approximately 1.7 to 1.8 Ga. Knowing that all of the cratonic sections were unified by approximately 1.7 Ga leads to the question of how and when these various terranes evolved prior to their amalgamation into Laurentia.

2. Materials and Methods

2.1. Location and Description of Samples

Zircon concentrates from seven samples were obtained from the Geological Survey of Canada. These include drill cores from the "PCA Home Pacific Knappen" (PCAPK), "Imperial Calstan Lake Newel" (ICLN), "PCA Calstan Parkland" (PCACP), and "PCP Medicine Hat Block" (PCPMB) wells [4]. Samples DRA-93-26, DRA-93-01, and DRA-93-20 are xenoliths from two localities in the Sweetgrass Hills, Coulee 29 minette [7,68] in the Milk River area of southern Alberta [69] and Sill 39 in northern Montana (Figure 1). Published U-Pb ages from Villeneuve et al. [4] and Davis et al. [5], analysis type, as well as sample descriptions are in Table 1.

Table 1. Published zircon U-Pb ages, analysis type, and sample descriptions of drill cores from Villeneuve et al. [4]. Published zircon U-Pb ages, analysis type, and sample descriptions of xenoliths are from Davis et al. [5].

	$^{207}Pb/^{206}Pb$	Analysis Type	Descriptions
	Age (Ga)		
Drill Core Samples [4]			
Home Pacific Knappen	3.278	single zircon core analysis	Banded greenish colored gneiss composed of quartz and feldspar with 20% biotite
Imperial Calstan Lake Newell	2.714	single zircon core analysis	Moderately fresh pegmatitic granodioritic gneiss composed of quartz, alkali feldspar, plagioclase, and hornblende with subordinate epidote and biotite
PCA Calstan Parkland	2.627	single zircon core analysis	Homogenous fresh medium- to fine-grained metabasite gneiss composed of biotite and plagioclase with subordinate hornblende
PCP Medicine Hat	2.7–2.8	single zircon core analysis	Massive, weakly foliated granitic gneiss that ranges in texture from medium-grained equigranular to pegmatitic and is cross-cut by chlorite-covered fractures

Table 1. *Cont.*

	$^{207}Pb/^{206}Pb$	Analysis Type	Descriptions
	Age (Ga)		
Xenolith Samples [5]			
DRA-93-26	2.65	not specified	Hornblende-biotite tonalite
DRA-93-01	1.72	multi-grain zircon U-Pb	Mafic granulite with a high-pressure assemblage (garnet–clinopyroxene–pigeonite–rutile +/− hornblende +/− quartz)
DRA-93-20	1.81	single zircon core analyses	Quartzo-feldspathic mesoperthite-rich granulite

2.2. U-Pb Geochronology of Zircon

Zircon grains provided by the Geological Survey of Canada were prepared using traditional methods of crushing and grinding, followed by density separation by panning, high-density liquids, and by magnetic susceptibility using a Frantz magnetic separator. Hand-picked zircon grains were embedded in a 25 mm epoxy disk, together with fragments of a natural zircon standard FC-1 [70–72]. The mounts were polished to approximately half thickness of the individual zircon grains, and imaged using cathodoluminescence (CL). In addition to the 484 U-Pb analyses, 106 Lu-Hf analyses were obtained from selected zircon domains identified in the CL images for each zircon. The zircon mounts were first analyzed for U-Pb, followed by Lu-Hf analysis in the same CL domain as the U-Pb analysis, but conducted in a separate session.

The U-Pb ages were determined using the Nu Plasma laser ablation-multi-collector-inductively coupled plasma mass spectrometry (LA-MC-ICP-MS) at the University of Florida (Gainesville, FL, USA) following methods in Mueller et al. [73]. The analyses utilized a New Wave 213 nm laser and a 20 µm spot diameter. Each individual U-Pb analysis consisted of 30 s of measurement during ablation in order to minimize ablation pit depth and elemental fractionation. Isotopic data were acquired using the Nu-Instruments Time Resolved Analysis software, which allowed isotopic ratios to be calculated from data collected simultaneously in individual faraday and ion-counting channels during the 30 s ablation. Fractionation and drift corrections were calibrated against multiple ablations of the FC-1 natural zircon standard (Duluth Gabbro; 1098 Ma; [70–72]); each batch of 10 unknowns was bracketed between two pairs of FC-1 analyses. The zircon isotopic data were reduced with the in-house program hosted in Microsoft Excel (CALAMARI, © P.A. Mueller), with ages and concordia diagrams calculated using Isoplot v. 4.0 [74,75]. Representative age errors based on the long-term reproducibility of FC-1 are 2% for $^{206}Pb/^{238}Pb$ (standard error of the mean (s.e.m.)) and 1% for $^{207}Pb/^{206}Pb$ (s.e.m.). U-Pb data, including for FC-1, are provided in the Supplementary Data (Tables S1 and S3).

2.3. Lu-Hf Isotopic Analysis of Zircon

Lu-Hf analyses were also conducted by laser ablation with the MC-ICP-MS in static mode following the methods in Mueller et al. [73]. Faraday collectors were used for the simultaneous measurement of ^{180}Hf, ^{178}Hf, ^{177}Hf, ^{176}Hf, ^{175}Lu, ^{174}Hf, and ^{172}Yb [73]. The analyses were performed with online Lu and Yb isobaric interference corrections, using $^{176}Lu/^{175}Lu = 0.02653$ and $^{176}Yb/^{172}Yb = 0.5870$, both of which are within the range of published values [76,77]. The non-radiogenic isotopic ratio of $^{180}Hf/^{177}Hf$ was measured to monitor mass bias corrections determined using $^{177}Hf/^{179}Hf$ and determined to be within the error of the true value (1.88710) for all unknowns and standards. Analyses that did not meet this criterion were discarded. Corrections for Lu and Yb interferences (peak stripping) were done on-line and based on mass bias-corrected ratios using the mass bias factors derived from Hf isotopes. This method was chosen because of the low reproducibility of Yb isotope ratios. Although mass bias for Yb, Lu, and Hf may have an elemental component to them, we do not utilize $^{176}Hf/^{177}Hf$ data that have combined Yb + Lu corrections in excess of 25%. Analyses with Yb + Lu corrections exceeding 20% are not used to define the limits of model ages or initial εHf for any suite of zircons. All Hf, Lu, and Yb isotopic

ratios were corrected for mass bias using $^{178}Hf/^{177}Hf = 1.46718$. Each analysis consisted of a 40 μm spot size and 20-s background measurement, up to one minute of measurement during ablation, and a 30-s purging period between analyses. Multiple analyses of FC-1 (Duluth Gabbro zircon standard; [71,78]) yielded $^{176}Hf/^{177}Hf = 0.28217$ (± 0.00002, 2σ, n = 9), which was within the error of solution analyses of this standard ($^{176}Hf/^{177}Hf = 0.282174 \pm 0.000013$, 2σ; [73]) as well as data published by Woodhead and Hergt (2005; $^{176}Hf/^{177}Hf = 0.282172 \pm 0.000042$, 2σ). The reproducibility of $^{176}Hf/^{177}Hf$ for FC-1 analyses in epsilon notation without age correction was −21.8 +/−1.1 εHf (2σ), which is within the error of reported values and the Florida lab's measurements of FC-1 by wet plasma [73,78]. The standard data were obtained during the same session as the unknown samples (1 standard, 15 unknowns, 1 standard). Measured and on-line mass-bias-corrected present-day $^{176}Lu/^{177}Hf$ ratios were utilized to calculate initial $^{176}Hf/^{177}Hf$ ratios using the decay constant of Lu ($\lambda = 1.867e^{-11}$; [79,80]) and the $^{207}Pb/^{206}Pb$ age of the analytical spot, following established procedures [81,82]. Overall, because of the very low Lu/Hf ratios (FC-1: $^{176}Lu/^{177}Hf = 0.001329 \pm 0.000091$, 2σ, n = 9), the difference between the present-day measured and calculated initial $^{176}Hf/^{177}Hf$ ratios in most cases is < 1 ε unit (e.g., [73]).

Zircons were selected for Lu-Hf analysis on the basis of low discordance (<10% $^{206}Pb/^{238}U$ versus $^{207}Pb/^{206}Pb$), zonation patterns, and grain size in order for the Lu-Hf analyses (40 μm spot) to be in the same domain as the U-Pb analysis (20 μm spot). Measuring Hf isotopes on the same zircons that are dated has the advantage of estimating the likelihood of open system behavior: Zircons that have experienced no, or only very little, Pb loss (i.e., concordant or nearly concordant) are the least likely to have suffered open system behavior of either Lu or Hf. The $^{176}Hf/^{177}Hf$ ratio is commonly represented as εHf, which is the $^{176}Hf/^{177}Hf$ in the unknown sample minus the $^{176}Hf/^{177}Hf$ in chondritic uniform reservoir, and then that value divided by $^{176}Hf/^{177}Hf$ in the chondritic uniform reservoir times 10,000 [83]. The chondritic uniform reservoir (CHUR) values are those of Bouvier et al. [84]: $^{176}Lu/^{177}Hf = 0.0336$ and $^{176}Hf/^{177}Hf = 0.282785$. Initial ratios are given as $^{176}Hf/^{177}Hf_{(T)}$ and $\varepsilon Hf_{(T)}$ for all analyzed samples and were calculated using the $^{207}Pb/^{206}Pb$ crystallization age of the zircon or its host rock and the measured Lu/Hf ratio, (e.g., initial Hf at 2.4 Ga = $\varepsilon Hf_{(2.4\ Ga)}$); propagated net uncertainties for initial ratios are approximately 1.5 ε-units (2σ) on average. On the basis of limited U-Pb age discordance, the initial Hf compositions likely reflect the composition of the magmas from which the zircons crystallized. Decay corrections are typically <1ε unit/b.y. in the case of Precambrian zircons. Depleted mantle (DM) model ages for FC-1 averaged 1.5 +/− 0.1 Ga (2σ) using the linear depleted mantle model from Mueller et al. [73]: $^{176}Hf/^{177}Hf = 0.0387$, εHf = 0.0 at 4.567 and 16 today) with propagated analytical errors only. The value of + 16 today for DM is within the range of values for modern Mid-Ocean Ridge Basalt (MORB) as summarized in Jones et al. [85] and Sanfilippo et al. [86]. The mean values for $^{176}Hf/^{177}Hf_{(T)}$ and $\varepsilon Hf_{(T)}$ (and related errors (± 2σ)) are summarized in Table 1; details of the specific grain analyses are available in Supplementary Table S2. FC-1 standard Lu-Hf isotopic data are available in Supplementary Data Table S4. Note that some grains were too small for both U-Pb and Lu- Hf analyses; only age data are reported for these grains.

In addition to providing insight into the role of mantle and crustal reservoirs in the development of the magmas from which the zircons crystallized, the range of initial εHf values can also be used to identify zircons that may not have crystallized from that magma, i.e., xenocrysts. Although there is no fixed range of initial εHf that can be used to constrain a felsic magma generated in a terrane with very old crust, the viability of the age can be enhanced if those ages lead to initial εHf values that cover a limited range and that range of values is comparable to the εHf values measured in the zircons today. The limits are unavoidably ad hoc to some degree, but comparisons with the ranges of initial εHf values determined for rocks of similar age in the region provide useful benchmarks. For example, the approximately 2.8 Ga Long Lake magmatic complex of the Beartooth Mountains has a range of initial εHf of 15 epsilon units [39,87], and the Paleoproterozoic igneous rocks of the Little Belt Mountains range over 23 epsilon units [88]. Measurement errors (i.e., ± 2σ) are inconsequential compared to the ranges of initial ratios.

3. Results

3.1. U-Pb Zircon Geochronology

Figure 2 shows representative CL images in which some grains show concentric, oscillatory zonation, which is characteristic of igneous zircon (HPK, #4 and DRA-93-26, #23) and unzoned or featureless outer domains (DRA-93-01, #35 and #39), which are interpreted as metamorphic overgrowths, while other grains appear to be completely featureless in CL (PCP-MHB).

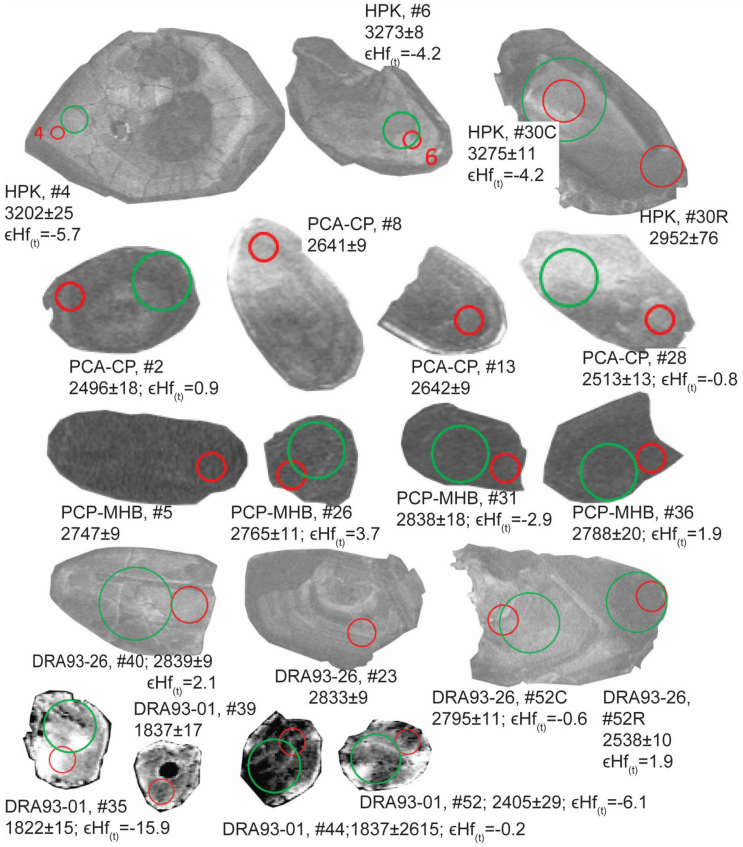

Figure 2. Representative CL images of analyzed zircon. Red smaller circles represent 20 μm U-Pb analysis spots. Green larger circles represent 40 μm Lu–Hf analysis spots.

Grains analyzed by ICP-MS for this study were selected from the zircon concentrates provided by the Geological Survey of Canada and previously described as part of earlier multi-grain ID-TIMS studies [4,5]. Here, individual analyses were first evaluated as acceptable if they met two criteria: (1) The $^{207}Pb/^{206}Pb$ age was < 5% discordant compared to the $^{206}Pb/^{238}U$ age, and (2) common Pb (i.e., mass ^{204}(Pb + Hg)) cps were less than the measured cps at mass 204 for the FC-1 standard. The values for ^{204}Pb cps and $^{204}Pb/^{206}Pb$ for the analyses and standards are available in the Supplementary Data. CA-TIMS analyses [72] showed that typical FC-1 zircons have $^{204}Pb/^{206}Pb < 0.001$. All analyses were plotted on a Tera-Wasserburg (TW) concordia diagram using the Isoplot program of Ludwig [74,75] to examine trends in discordance (Figures 3–5). The probability distribution function in Isoplot was used to identify age populations. Plots of $^{207}Pb/^{206}Pb$ ages versus percent discordance provided further insight into the behavior of age populations (Supplementary Table S1). These plots assisted in selecting grains for weighted average $^{207}Pb/^{206}Pb$ age calculations by clarifying relationships between age populations and discordance. Grains were selected based on their near concordance and limited range of $^{207}Pb/^{206}Pb$ ages as demonstrated within the plot. The calculation of a useful concordia intercept age was hindered in some samples by multi-stage Pb-loss. In these cases, we conducted a second evaluation (described

with each sample) and used error-weighted mean calculations (Isoplot v. 4.3, [74,75]) of low-discordance $^{207}Pb/^{206}Pb$ ages as the best minimum age estimate for the crystallization of the protolith. The external reproducibility of each individual zircon analysis ($^{207}Pb/^{206}Pb$ age) is approximately 1% (2σ) on the basis of reproducibility of the standard (FC-1; See Supplementary Data). Error error-weighted mean calculations [74,75] U-Pb age estimates (where applicable) are reported in Table 2.

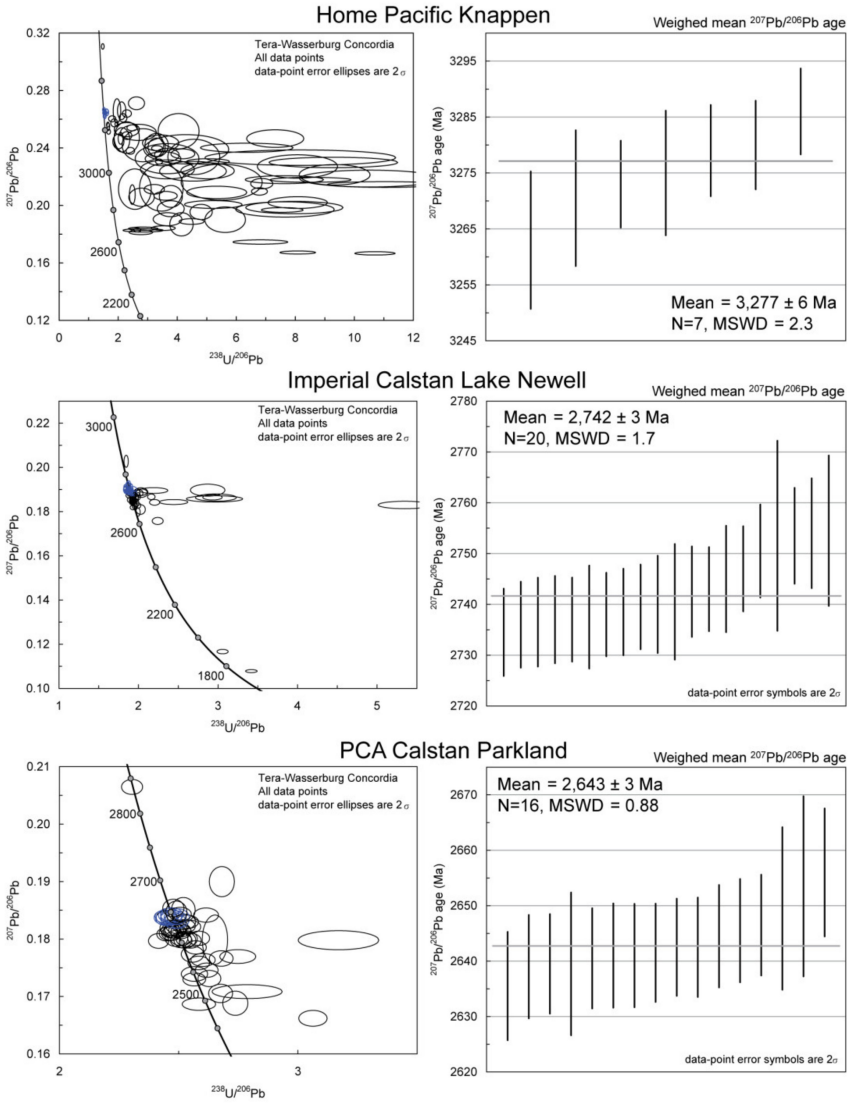

Figure 3. Unfiltered concordia plots of $^{207}Pb/^{206}Pb$ versus $^{238}U/^{206}Pb$ and corresponding ages showing the spread of zircons for samples analyzed in this study, and error-weighed mean $^{207}Pb/^{206}Pb$ ages Home Pacific Knapppen, PCA Castalan Parkland, and Imperial Castalan Lake Newel samples. The analyses used for the error-weighted mean calculations are highlighted in blue. Plots, ages, and age statistics are from Isoplot 3.7. See text for full discussion.

3.1.1. Home Pacific Knappen

Cathodoluminescence (CL) imaging revealed oscillatory zoned zircon grains typical of magmatic crystallization, with some grains exhibiting core-and-rim structures and fractures (Figure 2). Grains range in size from approximately 30 μm to 400 μm (long axis). Of the 90 analyses, discordance ranged to 90% (Supplementary Table S1). Seven low discordance grains (<5%) yielded an error-weighted mean age of 3.28 ± 0.01 Ga (MSWD = 2.3), which is interpreted as the age of protolith crystallization (Figure 3, Table 2).

Table 2. LA-ICP-MS data. $^{207}Pb/^{206}Pb$ ages and Lu–Hf-isotope data summarized.

	$^{207}Pb/^{206}Pb$	**Error**	**z/d/c [a]**	**$^{176}Hf/^{177}Hf$**	**$\varepsilon Hf_{(0)}$**	**$\varepsilon Hf_{(0)}$**	**$\varepsilon Hf_{(T)}$ [c]**	**$\varepsilon Hf_{(T)}$ [c]**	**Hf Model Age**
	Age (Ga)	2σ		(T) [b]	Range	Mean	Range	Mean	(Ga) (DM) [d]
Drill Core Samples									
Home Pacific Knappen	3.28	0.01	90/7/11	0.28054	−76.6 to −81.5	−78.2 ± 0.95	−3.1 to −8.7	−4.6 ± 1.1	3.62
Imperial Calstan Lake Newell	2.74	0.03	68/20/16	0.28112	−53.1 to −60.0	−58.3 ± 0.62	8.1 to 1.6	3.1 ± 0.61	2.86
PCA Calstan Parkland	2.64	0.02	60/16/13	0.28117	−51.0 to −58.5	−56.8 ± 0.83	8.5 to 1.1	2.5 ± 0.76	2.79
PCP Medicine Hat	N/A	N/A	70/NA/15	0.28103	−54.6 to −60.9	N/A	5.3 to −2.9 [e]	N/A	2.84 to 3.22
Xenolith Samples									
DRA-93-26	2.84	0.02	70/22/22	0.28101	−55.9 to −63.2	−61.4 ± 0.67	7.9 to 0.1	1.6 ± 0.64	3.01
DRA-93-01	1.81	0.05	59/16/16	0.28114	−56.5 to −63.9	−59.5 ± 1.0	−15.7 to −23.3	−17.0 ± 2.3	2.89
DRA-93-20	1.76	0.06	31/8/13	0.28125	−49.8 to −58.6	−53.6 ± 1.6	−10.1 to −20.1	−14.4 ± 1.8	2.69

[a] z/d; z, number of zircons analyzed for U–Pb per sample; d, number of zircon analyses used for age calculation; n, number of zircons analyzed for Lu–Hf per sample. [b] Error-weighted mean $^{176}Hf/^{177}Hf_{int}$ calculated by applying the ages given in $^{207}Pb/^{206}Pb$ Age (Ga) column. [c] εHf_T calculated by applying the ages given in $^{207}Pb/^{206}Pb$ Age (Ga) column, ± the standard deviation of the mean. [d] Depleted Mantle model ages were calculated using the model of Mueller et al. [73]. [e] εHf values were calculated using the individual U-Pb age for each grain.

3.1.2. Imperial Calstan Lake Newell

Zircon grains in this sample were mostly fragmented and dark in CL images, with limited observable zonation. Grains range in size from approximately 40 μm to 110 μm (long axis). The probability distribution function revealed two age populations in the total of 69 analyses: An older population of 31 grains at ca. 2.74 Ga, and a population of grains ≤ 2.7 Ga. The youngest two grains yielded ages of 1.76 ± 0.01 Ga and 1.91 ± 0.01 Ga, which may reflect zircon growth during later tectonothermal events [56]. The ca. 2.74 Ga analyses were further evaluated using the plots comparing percent discordance versus apparent $^{207}Pb/^{206}Pb$ ages grains, revealing a near concordant cluster of grains with discordance values between −2.1% and +2.2%, and $^{207}Pb/^{206}Pb$ ages from 2735 to 2755 Ma. This population of 20 grains yields an error-weighted mean age of 2.74 ± 0.03 (MSWD = 1.7; Figure 3, Table 2), which was interpreted as a crystallization age.

3.1.3. PCA Calstan Parkland

Most zircon grains in this sample are fragmented, but singly and doubly terminated grains are present as well. Grains range in size from approximately 60 to 200 μm (long axis). CL images reveal many grains with oscillatory growth zoning, in some cases also showing thin overgrowths or dark cores (Figure 2). Data were omitted based on the filtering criteria and occurrence along a Pb-loss trajectory observed on the concordia plot (Figure 3). The data were further evaluated in age versus percent discordance space, which revealed a population of grains with percent discordance values from −1.2 to + 0.9, and $^{207}Pb/^{206}Pb$ ages from 2634 to 2656 Ma. This population of 16 grains yield an error-weighted mean age of 2.64 ± 0.02 (MSWD = 0.88; Figure 3, Table 2). This age is interpreted as the minimum crystallization age, with the < 2.624 Ma ages possibly reflecting ancient Pb loss or total to partial metamorphic recrystallization.

3.1.4. PCP Medicine Hat

Zircon grains in this sample are often fragmented, but some elongate, rounded grains are present, ranging in size from approximately 50 to 170 μm (long axis). All grains were dark in CL images, with limited observable zonation (Figure 2). Out of the 70 individual zircon grains analyzed, only 11 pass the filtering criteria (Figure 4), and they range in age from approximately 2.70 to 2.78 Ga. This age distribution is interpreted to represent xenocrystic zircon in the protolith described as a granodiorite gneiss, with possible later overgrowths too small to be analyzed.

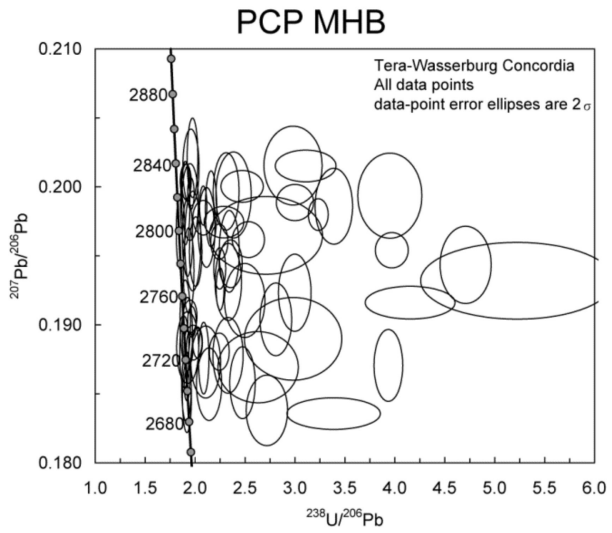

Figure 4. Unfiltered concordia plot and a probability distribution plot of filtered $^{207}Pb/^{206}Pb$ ages for sample PCP-Medicine Hat, showing the wide range of concordant analyses. See text for discussion.

3.1.5. DRA-93-26

Zircon grains from this xenolith include stubby, rounded morphologies and some blockier grain fragments, ranging in size from approximately 70 to 160 µm (long axis). CL images reveal apparent oscillatory zoned cores and unzoned dark CL overgrowths in some grains (Figure 2). Other grains display simpler oscillatory growth zoning (Figure 2). Many analyses that pass the filtering criteria lie on a discordia with intercepts at approximately 1.79 Ga and 2.86 Ga; however, no grains with $^{207}Pb/^{206}Pb$ ages older than 2.84 Ga are observed (Figure 5). The TW plot of this sample reveals an older age cluster at ca. 2.83 Ga, with a young tail (discordance >5%) trending down to approximately 2.45 Ga (Figure 5; Supplementary Table S1). We further evaluated analyses for an error-weighted mean age, favoring grains yielding percent discordance values between −1.6 and +2.5, and apparent $^{207}Pb/^{206}Pb$ ages ca. 2.82–2.84 Ga. The 22 grains passing these criteria yielded a $^{207}Pb/^{206}Pb$ age of 2.84 ± 0.02 Ga (MSWD = 1.2; Figure 5, Table 2). Younger, concordant ages from both cores and rims likely reflect Pb loss due to Paleoproterozoic tectonothermal event(s). The error-weighted mean age of 2.84 Ga is interpreted to be the best estimate of the minimum crystallization age of the protolith.

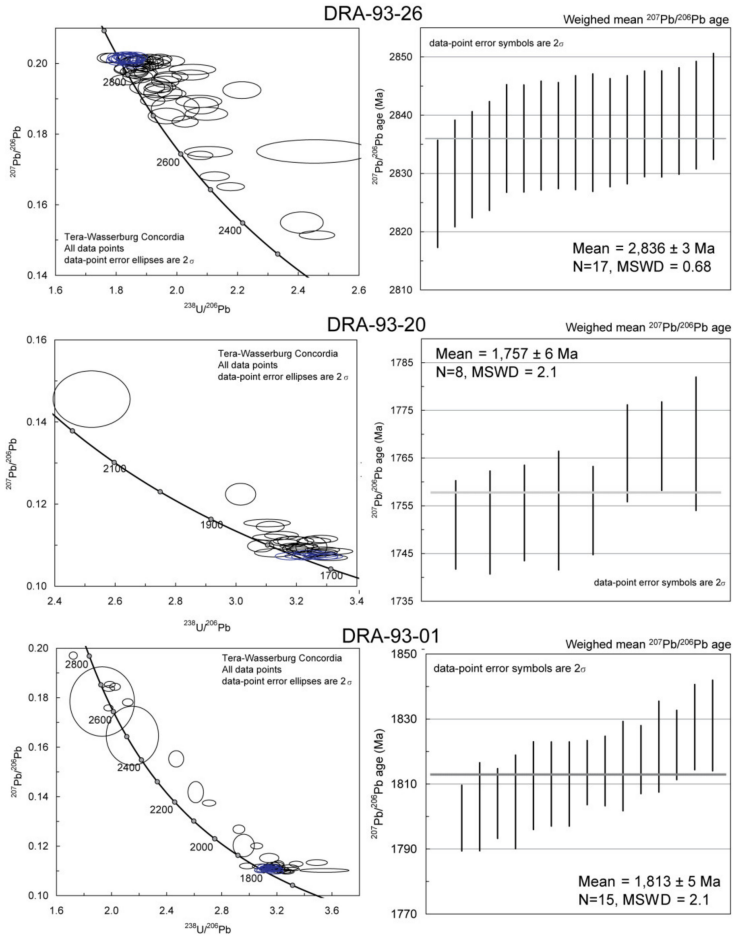

Figure 5. Unfiltered concordia plots of $^{207}Pb/^{206}Pb$ versus $^{238}U/^{206}Pb$ and corresponding ages showing the spread of zircon ages for samples analyzed in this study, and error-weighed mean $^{207}Pb/^{206}Pb$ ages for DRA-93-26, DRA-93-20, and DRA-93-01 samples. The analyses used for the error-weighted mean calculations are highlighted in blue. Plots, ages, and age statistics are from Isoplot 3.7. See text for full discussion.

3.1.6. DRA-93-01

Zircon grains from this xenolith are stubby to elongate, often with missing or rounded tips, ranging in size from approximately 50 to 180 µm (long axis). CL images reveal oscillatory growth zoning

that, in some cases, is overgrown by more homogenous rims (Figure 2). Thirteen of 59 analyses were rejected based on the initial filtering criteria. The three oldest concordant analyses from zircon cores yielding ages of ca. 2.69 Ga are interpreted as xenocrystic. The Paleoproterozoic aged analyses were further evaluated using plots comparing percent discordance versus apparent $^{207}Pb/^{206}Pb$ ages. We favored analyses yielding percent discordance values between −0.6 and +2.5. Sixteen analyses from zircon cores passed these secondary criteria, and 15 grains yielded an error-weighted mean age of 1.81 ± 0.05 Ga (MSWD = 2.1; Figure 5, Table 2). Petrographic analysis indicates a high-grade mineral assemblage (i.e., garnet–clinopyroxene–pigeonite–rutile +/− hornblende +/− quartz assemblage; [5,7,89]), suggesting that the original magma was emplaced into the lower crust (i.e., a charnockite).

3.1.7. DRA-93-20

Zircon grains from this xenolith are generally small and round to oval in shape, ranging in size from approximately 40 to 140 µm (long axis). CL images reveal small, oscillatory zoned cores in some grains, with thicker and rounder overgrowths. Other grains tend to show patchy zonation or little visible zonation. Four analyses were omitted based on the basic filtering criteria (Figure 5). Analyses were further evaluated using plots comparing percent discordance versus age (Supplementary Table S1). We favored analyses yielding percent discordance values between −1.2 and +2.5, and apparent $^{207}Pb/^{206}Pb$ ages ca. 1.75–1.78 Ga. The youngest coherent population of eight analyses passing these criteria were used to determine an error-weighted mean age of 1.76 ± 0.06 Ga (MSWD = 2.1; Figure 5, Table 2). This age is interpreted as the crystallization age for this sample.

3.2. Lu-Hf Zircon Isotope Geochemistry

Error-weighted mean $\varepsilon Hf_{(0)}$ (modern) and $\varepsilon Hf_{(T)}$ (ancient) values are available in Table 2. Individual grain $\varepsilon Hf_{(0)}$ and $\varepsilon Hf_{(T)}$ values are available in the Supplementary Data (Table S2). All $\varepsilon Hf_{(T)}$ data are plotted on Figure 6 versus the estimated crystallization age ($^{207}Pb/^{206}Pb$) of their host rock.

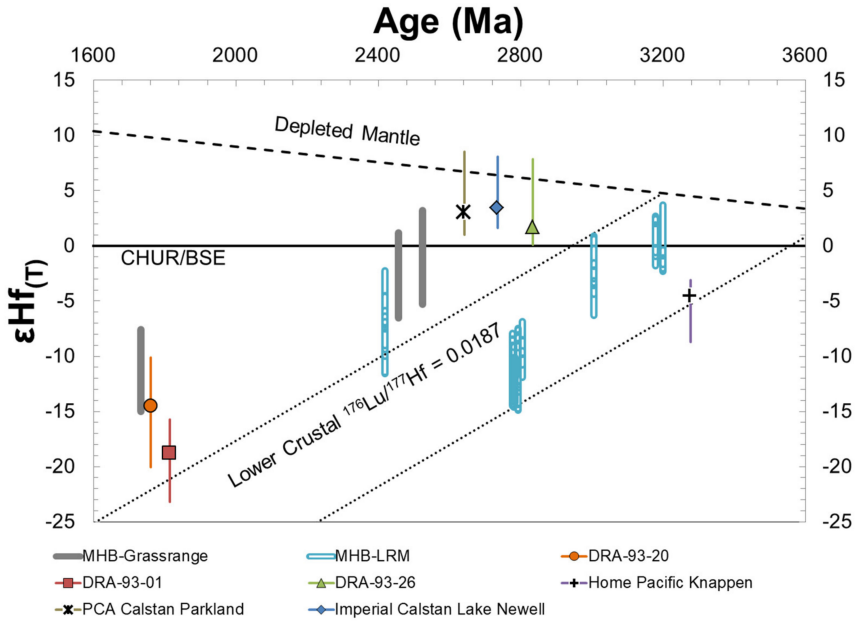

Figure 6. Lu-Hf evolution diagram showing the range for the drill core and xenolith samples. Lu-Hf data from xenoliths from the Medicine Hat block (MHB) are shown for comparison (thick gray bars; [56]). Lu-Hf data from the Little Rocky Mountains are shown for comparison (open bars; [57]). Evolution path based on lower crustal Lu/Hf ratios from Rudnick and Gao [90] (dotted lines). Symbols represent error-weighted means. CHUR: Chondritic Uniform Reservoir; BSE: Bulk Silicate Earth.

3.2.1. Home Pacific Knappen (HPK)

HPK yielded an error-weighted mean $\varepsilon Hf_{(0)}$ value of −78.2 ± 0.95 and a range of 4.9 ε-units, from −76.6 to −81.5 (n = 11). $\varepsilon Hf_{(3.3\ Ga)}$ values for the grains range from −3.1 to −8.7 (5.6 ε-units), with an error-weighted mean value of −4.6 ± 1.1 (Figure 6, Table 2).

3.2.2. Imperial Calstan Lake Newell (ICLN)

The error-weighted mean $\varepsilon Hf_{(0)}$ value for the data is −58.3±0.62, and the data range is a total of 6.9 ε-units, from −53.1 to −60.0 (n = 16). $\varepsilon Hf_{(2.7\ Ga)}$ defines a range from 8.1 to 1.6 (6.5 ε-units), with an error-weighted mean of 3.1 ± 0.61 (Figure 6, Table 2).

3.2.3. PCA Calstan Parkland (PCACP)

PCACP yielded an error-weighted mean $\varepsilon Hf_{(0)}$ value of −56.8 ± 0.83 and a range of 7.5 ε-units, from −51.0 to −58.5 (n = 13). $\varepsilon Hf_{(2.6\ Ga)}$ for the grains range from 8.5 to 1.1 (7.4 ε-units), with an error-weighted mean value of 2.5 ± 0.76 (Figure 6, Table 2).

3.2.4. PCP Medicine Hat (PCPMH)

The sample yielded $\varepsilon Hf_{(0)}$ values ranging from −54.6 to −60.9 (n = 15; 6.3 ε-unit range) (Table 2). Due to the lack of a coherent crystallization age for this sample, $\varepsilon Hf_{(T)}$ values are calculated to the individual zircon age. These values range from −2.9 to 5.3 (8.2 ε-unit range).

3.2.5. DRA-93-26

The zircons yielded an error-weighted mean $\varepsilon Hf_{(0)}$ value of −61.4 ± 0.67, ranging from −55.9 to −63.2 (n = 22; 7.3 ε-units) and $\varepsilon Hf_{(2.8\ Ga)}$ define a range from 7.9 to 0.1 (7.8 ε-units), with an error-weighted mean of 1.6 ± 0.64 (Figure 6, Table 2).

3.2.6. DRA-93-01

The sample showed an error-weighted mean $\varepsilon Hf_{(0)}$ value of −59.5 ± 1.0 ranging from −50.8 to −63.9 (n = 16; 13.1 ε-unit range). When $\varepsilon Hf_{(1.8\ Ga)}$ was calculated, the $\varepsilon Hf_{(1.8\ Ga)}$ values range from −15.7 to −23.2 (7.5 ε-units), with an error-weighted mean value of −17.0 ± 2.3 (Figure 6, Table 2).

3.2.7. DRA-93-20

$\varepsilon Hf_{(0)}$ values yielded an error-weighted mean of −53.6 ± 1.6 ranging from −49.8 to −58.6 (n = 13; 8.8 ε-units), and $\varepsilon Hf_{(1.8\ Ga)}$ define a range from −10.1 to −20.1 (10 ε-units), with an error-weighted mean of −14.4 ± 1.8 (Figure 6, Table 2).

4. Discussion

The new, single grain U–Pb zircon ages presented here largely support previous multi-grain analyses, mostly concordia upper intercept ages, reported by Villeneuve et al. [4] and Davis et al. [5] for the same zircon concentrates. The Home Pacific Knappen core yields zircons with reliable ages of approximately 3.28 Ga, while the remainder of the samples yielded slightly older ages than previously cited (Tables 1 and 2), with the exception of DRA-93-20, which yielded a slightly younger age than previously published (Tables 1 and 2; [4,5]). Collectively, the Archean crystallization ages presented here and by Davis et al. [5] and in other samples analyzed by Villeneuve et al. [4] confirm the widespread presence of Mesoarchean crust in the MHB and southern Hearne Province.

Whole-rock Sm-Nd isotopes of two samples discussed in Villeneuve et al. [4] yielded initial εNd values of + 0.6 and −0.1 (PCP Travers and HPK respectively), crustal residence, or mantle extraction ages of 2.86 and 3.48 Ga, respectively, and $^{147}Sm/^{144}Nd$ ratios not typical of continental crust ($^{147}Sm/^{144}Nd$ = 0.1532; [90]). The Sm–Nd isotopic data of Villeneuve et al. [4] are similar to the data

of Frost and Burwash [91] for the MHB and southern Hearne Province with crustal residence ages ranging from approximately 2.6 Ga to 3.2 Ga [91] and a range (−4.04 to −12.8; [91]) of $\varepsilon Nd_{1.8\ Ga}$ values.

In terms of Hf isotopes, Archean samples show a mixture of initial Hf isotopic values ranging from positive depleted mantle values to CHUR/BSE values (Figure 6; $\varepsilon Hf_{(T)}$ = 8.5 to 0.1). These values indicate that mantle-derived melts invariably interacted with older, more heterogeneous crust to yield the range of observed $Hf_{(T)}$ values. The age estimates for this older crust (approximately 2.8 Ga to 3.6 Ga) are based on the lower crustal Lu–Hf ratio ($^{176}Lu/^{177}Hf$ = 0.0187) shown in Figure 6; current ratios, as well as depleted mantle model ages, are shown in Table 2. There is evidence in the Lu/Hf ratios of the Mesoarchean zircons, albeit limited, of Archean crust with components >3.2 Ga within the MHB (Figure 6; this study; [4,5,56,57]), which indicates that there might be parts of the MHB not yet discovered that record an older history. These possible exceptions aside, the data summarized here strongly suggest that the MHB is similar to other Archean provinces around the world in containing a large amount of crust created between approximately 2.8 and 2.5 Ga [4,5,66]. This conclusion is compatible with interpretations of extant whole rock Sm-Nd isotopic data that yield Archean crustal residence ages for all of the xenoliths and basement cores discussed here and elsewhere [4,5,91]. Similarly, εHf values of zircons for the drill cores and xenoliths range from DM to more negative epsilon values, indicating the mixing and reworking of older crustal materials. The Lu-Hf T_{DM} of approximately 3.6 Ga for zircons from the HPK core (Table 2) indicates that older material equivalent to the MMT [32,92–94] was likely present in the MHB during development of the Neoarchean and Paleoproterozoic crust. This buried Meso- to Paleoarchean crust is a good candidate for the older contaminating component that contributed to lowering the εHf values of the Neoarchean samples (e.g., Figure 6 lower crustal evolution path). Similarly, the Sm-Nd isotopic values for the Mesoarchean MMT crust also involve the mixing of juvenile and older crustal material, although showing a larger range in ε-units (approximately 8.5 Nd ε-units; + 4.9 εNd to −4.3 εNd_T values [49,95]).

Although the extent of the Wyoming province, Medicine Hat block, and Hearne provinces and their temporal relationships to the Superior Province across the Trans-Hudson orogen are still debated, the similarity of ages and isotopic compositions between the MHB and the northern Wyoming Province, particularly the MMT, suggests that these two terranes may have shared at least a partial history (Figure 7A). If so, the MMT–MHB connection likely existed as far back as the Mesoarchean, strengthening proposals for a connection between the MHB and Wyoming Province [6]. The connection was likely broken sometime during the earliest Paleoproterozoic with the formation of a small ocean basin (Medicine Hat ocean) that separated the MMT and other parts of the northern Wyoming Province from the MHB and possibly related terranes such as the Clearwater and Priest River (e.g., [96–99]). Closure of this ocean by north dipping subduction [28] led to the formation of the Little Belt continental arc on MHB crust beginning at approximately 1.9 Ga [58]. The MHB and MMT re-joined at this time as they amalgamated into the supercontinent Laurentia during the Great Falls orogeny (1.7–1.9 Ga), which formed the GFTZ [1,28,56–59]. The GFTZ developed in the same timeframe as the better known Trans-Hudson orogen [60–67] to the east that marks the merger of the Wyoming, Hearne, and Superior Provinces, which along with the MHB formed the Archean core of western Laurentia. The impetus for closure of the Medicine Hat ocean, formation of the GFTZ, and amalgamation of the Superior, Hearne, and Wyoming Provinces remains unclear, but the presence of the approximately 1.8 Ga Rimbey arc immediately northwest of the MHB/Vulcan zone and its proposed relation to the collision of Australia and Laurentia (e.g., [100,101]) coincides with ages presented here and high-grade 1.75–1.85 metamorphism of the western Hearne Province [102]. This collisional scenario is complex and associated with the formation of Nuna-Columbia. Although there are several extant proposals for the sequence of events that led to the formation of a combined Nuna-Columbia-Laurentia scale supercontinent in the Paleoproterozoic, many authors have proposed that a firm connection was established between Laurentia and Australia in the interval 1.8–1.6 Ga (e.g., [103–105]). Establishing this connection involved at least one continent–continent or craton–craton collision, which would be of

the appropriate scale to induce a wide area of modern northwestern North America characterized by 1.7–1.8 Ga magmatic crystallization ages and metamorphic cooling ages.

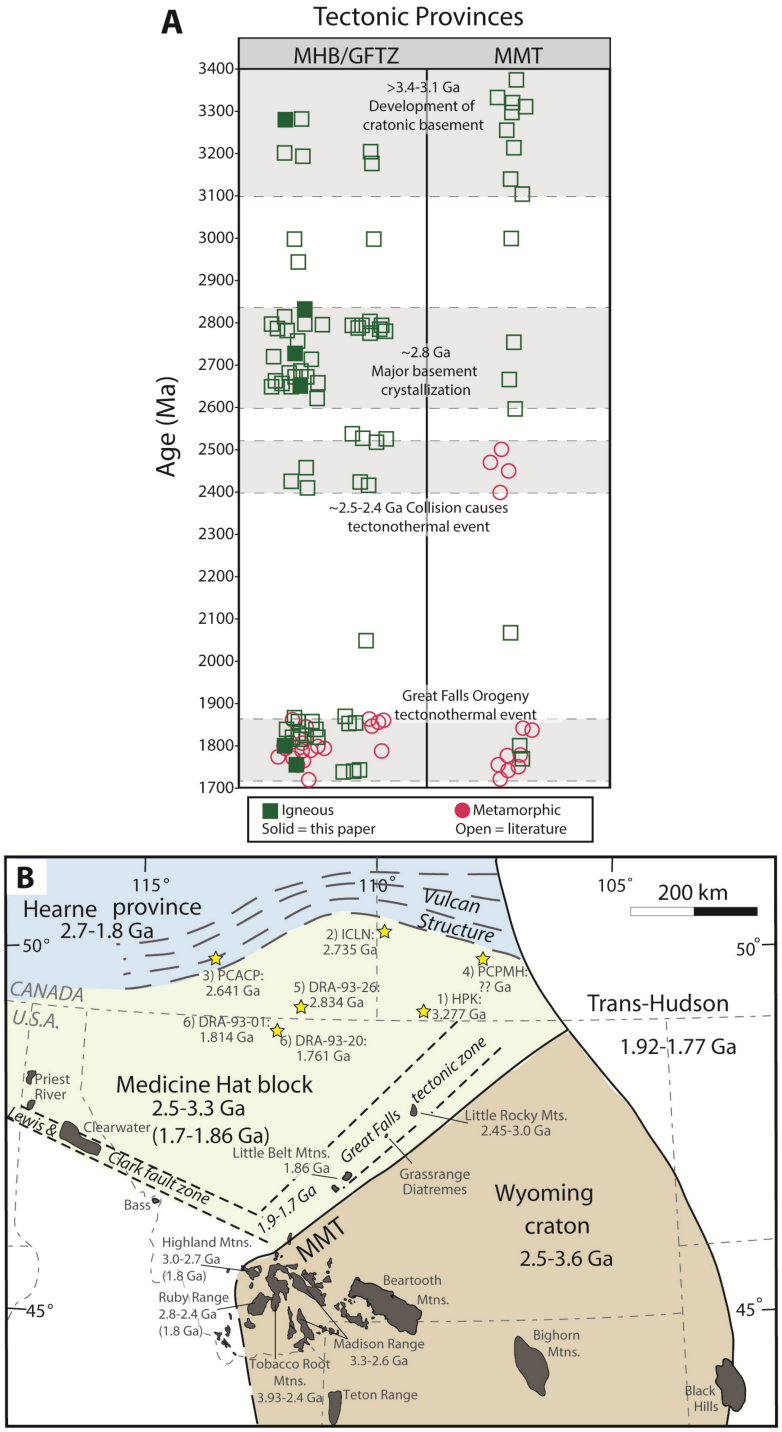

Figure 7. (**A**) Published Archean to Paleoproterozoic U-Pb ages of zircons from the Montana Metasedimentary terrane (MMT: Ruby Range, Tobacco Root Mountains, Madison Range, Highland Mountains: [32,49,94,95,106–108]). Published ages for the Medicine Hat block and Great Falls tectonic zone (MHB/GFTZ: drill cores, Sweetgrass Hills xenoliths, Priest River Complex, Clearwater Complex, Little Belt Mountains, Little Rocky Mountains, Grassrange Diatreme xenoliths, this study; [4,5,56–59,95,98,99], all of which is being reported here. For reference, ages are plotted compared to U-Pb ages from this study. Ages interpreted as times of igneous crystallization are represented as squares, and potential

metamorphic ages are represented as circles. Ages from this study are solid symbols, and ages from the literature are open symbols. (**B**) The approximate locations and relative positions of the Wyoming Province, MHB, Hearne Province, GFTZ (tightly dashed lines), Trans-Hudson, and Vulcan low (represented by the widely spaced waved lines) [14,24,25,91,109] with corresponding ages cited above.

5. Conclusions

The data presented here help expand our understanding of the age and tectonic evolution of the largely concealed Medicine Hat block. The new U-Pb ages presented generally agree with previous Archean and Paleoproterozoic age determinations for the region [4,5]; however, they help resolve complexities caused by discordance only hinted at by previous analyses of these samples. The ages generated in this study tend to be slightly older than the earlier multi-grain analyses, which may have been more affected by Pb loss or the incorporation of later metamorphic zircon growth in multi-grain dissolutions. Lu-Hf isotopic analyses paired with single-grain U-Pb data help further constrain the crustal evolution of the MHB, reinforcing that it contains a large amount of crust created between approximately 2.8 and 2.5 Ga. The initial εHf values for the majority of the samples from this study range from DM, indicating juvenile materials, mixed with reworked older Meso- to Paleoarchean crustal materials. The samples reveal similarities to the ages and isotopic compositions of the MMT, suggesting a connection between the MHB and the MMT in their history. This connection was likely broken sometime in the earliest Paleoproterozoic, leading to the formation of a small ocean basin that later closed, resulting in the Little Belt continental arc at approximately 1.9 Ga. The prevalence of Paleoproterozoic ages across the MHB, GFTZ, and MMT (approximately 1.9 Ga to 1.7 Ga) record the entire Great Falls Orogeny, and time that the combined MHB-WY-Hearne crust was amalgamated with the Superior Province to form the Archean core of Laurentia.

Supplementary Materials: The following are available online at http://www.mdpi.com/2076-3263/10/7/271/s1, Table S1: U-Pb zircon geochronologic analyses. Table S2: Lu-Hf zircon isotope geochemical analyses. Table S3: FC-1 standard U-Pb zircon analyses. Table S4: FC-1 standard Lu-Hf isotope geochemical analyses.

Author Contributions: Conceptualization, J.N.G.; Formal analysis, J.N.G. and S.J.M.; Funding acquisition, J.N.G.; Investigation, J.N.G.; Methodology, J.N.G.; Project administration, J.N.G.; Resources, J.N.G.; Validation, J.N.G., S.J.M. and P.A.M.; Visualization, J.N.G. and S.J.M.; Writing—original draft, J.N.G. and S.J.M.; Writing—review and editing, J.N.G., S.J.M. and P.A.M. All authors have read and agreed to the published version of the manuscript.

Funding: This research was funded by The University of Mississippi Department of Geology and Geological Engineering.

Acknowledgments: We wish to thank William (Bill) Davis from the Geological Survey of Canada for allowing us to work on the samples. George Kamenov is gratefully acknowledged for all of his help with attaining the U–Pb and Lu–Hf analyses for this project.

Conflicts of Interest: The authors declare no conflict of interest. The funders had no role in the design of the study; in the collection, analyses, or interpretation of data; in the writing of the manuscript, or in the decision to publish the results.

References

1. O'Neill, J.M.; Lopez, D.A. Character and regional significance of the Great Falls tectonic zone, east-central Idaho and west-central Montana. *Am. Assoc. Pet. Geol. Bull.* **1985**, *69*, 437–447.
2. Ross, G.M. Precambrian basement in the Canadian Cordillera: An introduction. *Can. J. Earth Sci.* **1991**, *28*, 1133–1139. [CrossRef]
3. Pilkington, M.; Grieve, R.A.F.; Rupert, J.D.; Halpenny, J.F. Gravity anomaly map with shaded relief of gradient of North America. *Geol. Surv. Can.* **1992**, Map 1807A, scale 1:10,000,000. [CrossRef]
4. Villeneuve, M.E.; Ross, G.M.; Thériault, R.J.; Miles, W.; Parrish, R.R.; Broome, J. Tectonic subdivision and U-Pb geochronology of the crystalline basement of the Alberta Basin, Western Canada. *Geol. Surv. Can. Bull.* **1993**, *447*, 86.

5. Davis, W.J.; Berman, R.; Kjarsgaard, B. U-Pb Geochronology and Isotopic Studies of Crustal Xenoliths from the Archean Medicine Hat Block, Northern Montana and Southern Alberta: Paleoproterozoic Reworking of Archean Lower Crust. *Lithoprobe* **1995**, *47*, 329–334.
6. Buhlmann, A.L.; Cavell, P.; Burwash, R.A.; Creaser, R.A.; Luth, R.W. Minette bodies and cognate mica-clinopyroxenite xenoliths from the Milk River area, southern Alberta: Records of a complex history of the northernmost part of the Archean Wyoming craton. *Can. J. Earth Sci.* **2000**, *37*, 1629–1650. [CrossRef]
7. Collerson, K.D.; Hearne, B.C.; Macdonald, R.A.; Upton, B.G.J.; Park, J.G. Granulite xenoliths from the Bearpaw Mountains, Montana: Contraints on the character and evolution of lower continental crust. *Terra Cogn.* **1988**, *8*, 270.
8. Ross, G.M. Introduction to special issue of Canadian Journal of Earth Sciences: The Alberta Basement Transect of Lithoprobe. *Can. J. Earth Sci.* **2002**, *39*, 287–288. [CrossRef]
9. Ross, G.M.; Parrish, R.R.; Villeneuve, M.E.; Bowring, S.A. Geophysics and geochronology of the crystalline basement of the Alberta basin, western Canada. *Can. J. Earth Sci.* **1991**, *28*, 512–522. [CrossRef]
10. Pilkington, M.; Miles, W.F.; Ross, G.M.; Roest, W.R. Potential-field signatures of buried Precambrian basement in the Western Canada Sedimentary Basin. *Can. J. Earth Sci.* **2000**, *37*, 1453–1471. [CrossRef]
11. Ross, D.J.K.; Bustin, R.M. Characterizing the shale gas resource potential of Devonian-Mississippian strata in the Western Canada sedimentary basin: Application of an integrated formation evaluation. *Am. Assoc. Pet. Geol. Bull.* **2008**, *92*, 87–125. [CrossRef]
12. Ross, G.M.; Milkereit, B.; Eaton, D.; White, D.; Kanasewich, E.R.; Burianyk, M.J.A. Paleoproterozoic collisional orogen beneath the Western Canada Sedimentary Basin imaged by Lithoprobe crustal seismic-reflection data. *Geology* **1995**, *23*, 195–199. [CrossRef]
13. Peterman, Z.E. Dating of Archean basement in northeastern Wyoming and southern Montana. *GSA Bull.* **1981**, *92*, 139–146. [CrossRef]
14. Hoffman, P.F. United plates of America, the birth of a craton: Early Proterozoic assembly and growth of Laurentia. *Annu. Rev. Earth Planet. Sci.* **1988**, *16*. [CrossRef]
15. Collerson, K.D.; Hearn, B.C.; Macdonald, R.A.; Upton, B.G.J.; Harmon, R.S. Composition and evolution of lower continental crust: Evidence from xenoliths in Eocene lavas from the Bearpaw Mountains, Montana. *Abstr. Int. Assoc. Volcanol. Chem. Earth's Inter. Gen. Assem.* **1989**, *131*, 57.
16. Condie, K.C. Introduction. In *Developments in Precambrian Geology*; Elsevier: Amsterdam, The Netherlands, 1992.
17. Doughty, P.T.; Price, R.A.; Parrish, R.R. Geology and U-Pb geochronology of Archean basement and Proterozoic cover in the Priest River complex, northwestern United States, and their implications for Cordilleran structure and Precambrian continent reconstructions. *Can. J. Earth Sci.* **1998**, *35*, 39–54. [CrossRef]
18. Foster, D.A.; Mueller, P.A.; Mogk, D.W.; Wooden, J.L.; Vogl, J.J. Proterozoic evolution of the western margin of the Wyoming craton: Implications for the tectonic and magmatic evolution of the northern Rocky Mountains. *Can. J. Earth Sci.* **2006**, *43*, 1601–1619. [CrossRef]
19. Foster, D.A.; Mueller, P.A.; Heatherington, A.; Gifford, J.N.; Kalakay, T.J. Lu-Hf systematics of magmatic zircons reveal a Proterozoic crustal boundary under the Cretaceous Pioneer batholith, Montana. *Lithos* **2012**, *142–143*, 216–225. [CrossRef]
20. Klasner, J.S.; King, E.R. Precambrian basement geology of North and South Dakota. *Can. J. Earth Sci.* **1986**, *23*, 1083–1102. [CrossRef]
21. Lewry, J.F.; Stauffer, M.R. The Early Proterozoic Trans-Hudson Orogen of North America. *Geol. Assoc. Can. Spec. Pap.* **1990**, *37*, 505.
22. Baird, D.J.; Nelson, K.D.; Knapp, J.H.; Walters, J.J.; Brown, L.D. Crustal structure and evolution of the Trans-Hudson orogen: Results from seismic reflection profiling. *Tectonics* **1996**, *15*, 416–426. [CrossRef]
23. Mueller, P.; Mogk, D.; Wooden, J.; Spake, D. U-Pb ages of zircons from the Lower Belt Supergroup and proximal crystalline basement: Implications for the early evolution of the Belt Basin. *Spec. Pap. Geol. Soc. Am.* **2016**, *522*, 283–303. [CrossRef]
24. Mueller, P.A.; Burger, H.R.; Wooden, J.L.; Brady, J.B.; Cheney, J.T.; Harms, T.A.; Heatherington, A.L.; Mogk, D.W. Paleoproterozoic Metamorphism in the Northern Wyoming Province: Implications for the Assembly of Laurentia. *J. Geol.* **2005**, *113*, 169–179. [CrossRef]
25. Mueller, P.A.; Frost, C.D. The Wyoming Province: A distinctive Archean craton in Laurentian North America. *Can. J. Earth Sci.* **2006**, *43*, 1391–1397. [CrossRef]

26. Henstock, T.J.; Levander, A.; Snelson, C.M.; Keller, G.R.; Miller, K.C.; Harder, S.H.; Gorman, A.R.; Clowes, R.M.; Burianyk, M.J.A.; Humphreys, E.D. Probing the Archean and Proterozoic lithosphere of western North America. *GSA Today* **1998**.
27. Boerner, D.E.; Craven, R.D.; Kurtz, R.D.; Ross, G.M.; Jones, F.W. The Great Falls Tectonic Zone: Suture or intracontinental shear zone? *Can. J. Earth Sci.* **1998**, *35*, 175–183. [CrossRef]
28. Gorman, A.R.; Clowes, R.M.; Ellis, R.M.; Henstock, T.J.; Spence, G.D.; Keller, G.R.; Levander, A.; Snelson, C.M.; Burianyk, M.J.; Kanasewich, E.R.; et al. Deep Probe: Imaging the roots of western North America. *Can. J. Earth Sci.* **2002**, *39*, 375–398. [CrossRef]
29. Mogk, D.W.; Henry, D.J. Metamorphic petrology of the northern Archean Wyoming province. southwestern Montana: Evidence for Archean collisional tectonics. In *Metamorphism and Crustal Evolution in the Western U.S.*; Ernst, W.G., Ed.; Prentice-Hall: Upper Saddle River, NJ, USA, 1988; pp. 363–382.
30. Erslev, E.A.; Sutter, J.F. Evidence for Proterozoic mylonitization in the northwestern Wyoming province. *Geol. Soc. Am. Bull.* **1990**, *102*, 1681–1694. [CrossRef]
31. Mogk, D.W.; Mueller, P.A.; Wooden, J.L. The nature of Archean terrane boundaries: An example from the northern Wyoming Province. *Precambrian Res.* **1992**, *55*, 155–168. [CrossRef]
32. Mueller, P.A.; Shuster, R.D.; Wooden, J.L.; Erslev, E.A.; Bowes, D.R. Age and composition of Archean crystalline rocks from the southern Madison Range, Montana: Implications for crustal evolution in the Wyoming craton. *Geol. Soc. Am. Bull.* **1993**, *105*, 437–446. [CrossRef]
33. Mueller, P.A.; Wooden, J.L.; Nutman, A.P.; Mogk, D.W. Early Archean crust in the northern Wyoming province Evidence from U-Pb ages of detrital zircons. *Precambrian Res.* **1998**, *91*, 295–307. [CrossRef]
34. Wooden, J.L.; Mueller, P.A. Pb, Sr, and Nd isotopic compositions of a suite of Late Archean, igneous rocks, eastern Beartooth Mountains: Implications for crust-mantle evolution. *Earth Planet. Sci. Lett.* **1988**, *87*, 59–72. [CrossRef]
35. Chamberlain, K.R.; Frost, C.D.; Frost, B.R. Early Archean to Mesoproterozoic evolution of the Wyoming Province: Archean origins to modern lithospheric architecture. *Can. J. Earth Sci.* **2003**, *40*, 1357–1374. [CrossRef]
36. Harms, T.A.; Brady, J.B.; Burger, H.R.; Cheney, J.T. Advances in the geology of the Tobacco Root Mountains, Montana, and their implications for the history of the northern Wyoming province. *Spec. Pap. Geol. Soc. Am.* **2004**, *377*, 227–243. [CrossRef]
37. Jones, C.L. U-Pb Geochronology of Monazite and Zircon in Precambrian Metamorphic Rocks from the Ruby Range, SW Montana: Deciphering Geological Events that Shaped the NW Wyoming Province. Master's Thesis, Kent State University, Kent, OH, USA, 2008; 131p.
38. Alcock, J.; Mueller, P.A. A Paleoproterozoic sedimentary basin within the Wyoming Craton exposed in the Ruby Range, SW Montana. *Northwest Geol.* **2012**, *41*, 47–62.
39. Condit, C.B.; Mahan, K.H.; Ault, A.K.; Flowers, R.M. Foreland-directed propagation of high-grade tectonism in the deep roots of a Paleoproterozoic collisional orogen, SW Montana, USA. *Lithosphere* **2015**, *7*, 625–645. [CrossRef]
40. Mueller, P.A.; Wooden, J.L. Trace Element and Lu-Hf Systematics in Hadean-Archean Detrital Zircons: Implications for Crustal Evolution. *J. Geol.* **2012**, *120*, 15–29. [CrossRef]
41. Mueller, P.A.; Cordua, W.S. Rb-Sr whole rock age of gneisses from the Horse Creek area, Tobacco Root Mountains, Montana. *Isochron/West* **1976**, *16*, 33–36.
42. James, H.L.; Hedge, C.E. Age of the basement rocks of southwest Montana. *Geol. Soc. Am. Bull.* **1980**, *91*, 11–15. [CrossRef]
43. Salt, K.J. Archean Geology of the Spanish Peaks Area, Southwestern Montana. Master's Thesis, Montana State University, Bozeman, MT, USA, 1987; pp. 1–81.
44. Weyand, E.L. U-Pb Zircon Geochronology of Archean Rocks from the Spanish Peaks Area, Madison Range, Montana. Ph.D. Thesis, University of Florida, Gainesville, FL, USA, 1989.
45. Kellogg, K.S.; Mogk, D.W. Structural development of high-temperature mylonites in the Archean Wyoming province, northwestern Madison Range, Montana. *Rocky Mt. Geol.* **2009**, *44*, 85–102. [CrossRef]
46. Mueller, P.A.; Wooden, J.L. Evidence for Archean subduction and crustal recycling, Wyoming province. *Geology* **1988**, *16*, 871–874. [CrossRef]
47. Roberts, H.; Dahl, P.; Kelley, S.; Frei, R. New 207Pb-206Pb and 40Ar-39Ar ages from SW Montana, USA: Constraints on the Proterozoic and Archæan tectonic and depositional history of the Wyoming province. *Precambrian Res.* **2002**, *117*, 119–143. [CrossRef]

48. Cheney, J.T.; Webb, A.A.G.; Coath, C.D.; McKeegan, K.D. In situ ion microprobe 207Pb/206Pb dating of monazite from Precambrian metamorphic suites, Tobacco Root Mountains, Montana. *Spec. Pap. Geol. Soc. Am.* **2004**, *377*, 151–179. [CrossRef]
49. Mueller, P.A.; Burger, H.R.; Wooden, J.L.; Heatherington, A.L.; Mogk, D.W.; D'Arcy, K. Age and evolution of the Precambrian crust of the Tobacco Root Mountains, Montana. *Spec. Pap. Geol. Soc. Am.* **2004**, *377*, 181–202. [CrossRef]
50. Harlan, S.S.; Geissman, J.W.; Snee, L.W.; Reynolds, R.L. Late Cretaceous remagnetization of Proterozoic mafic dikes, southern Highland Mountains, southwestern Montana: A paleomagnetic and 40Ar/39Ar study. *Bull. Geol. Soc. Am.* **1996**, *108*, 653–668. [CrossRef]
51. O'Neill, J.M. The Great Falls Tectonic Zone, Montana-Idaho: An Early Proterozoic collisional orogen beneath and south of the Belt Basin. In *Belt Symposium III*; Montana Bureau of Mines and Geology: Butte, MT, USA, 1998; Volume 112, pp. 222–228.
52. Condit, C.B.; Mahan, K.H.; Curtis, K.C.; Möller, A. Dating metasomatism: Monazite and zircon growth during amphibolite facies albitization. *Minerals* **2018**, *8*, 187. [CrossRef]
53. Ault, A.K.; Flowers, R.M.; Mahan, K.H. Quartz shielding of sub-10µm zircons from radiation damage-enhanced Pb loss: An example from a metamorphosed mafic dike, northwestern Wyoming craton. *Earth Planet. Sci. Lett.* **2012**, *339–340*, 57–66. [CrossRef]
54. Spencer, E.W.; Kozak, S.J. Precambrian evolution of the Spanish Peaks Area, Montana. *Bull. Geol. Soc. Am.* **1975**, *86*, 785–792. [CrossRef]
55. Alcock, J.; Muller, P.D.; Jercinovic, M.J. Monazite ages and pressure-temperature-time paths from anatectites in the southern Ruby Range, Montana, USA: Evidence for delamination, ultramafic magmatism, and rapid uplift at ca. 1780 Ma. *Can. J. Earth Sci.* **2013**, *50*, 1069–1084. [CrossRef]
56. Gifford, J.N.; Mueller, P.A.; Foster, D.A.; Mogk, D.W. Precambrian Crustal Evolution in the Great Falls Tectonic Zone: Insights from Xenoliths from the Montana Alkali Province. *J. Geol.* **2014**, *122*, 531–548. [CrossRef]
57. Gifford, J.N.; Mueller, P.A.; Foster, D.A.; Mogk, D.W. Extending the realm of Archean crust in the Great Falls tectonic zone: Evidence from the Little Rocky Mountains, Montana. *Precambrian Res.* **2018**, *315*, 264–281. [CrossRef]
58. Mueller, P.A.; Heatherington, A.L.; Kelly, D.M.; Wooden, J.L.; Mogk, D.W. Paleoproterozoic crust within the Great Falls tectonic zone: Implications for the assembly of southern Laurentia. *Geology* **2002**, *30*, 127–130. [CrossRef]
59. Mueller, P.A.; Heatherington, A.L.; Mogk, D.W.; Wooden, J.L. Paleoproterozoic tectonothermal activity along the NW margin of the Archean Wyoming province. *Geol. Soc. Am. Abstr. Programs* **1999**, *31*, A107.
60. Ansdell, K.M. Tectonic evolution of the Manitoba-Saskatchewan segment of the Paleoproterozoic Trans-Hudson Orogen, Canada. *Can. J. Earth Sci.* **2005**, *42*, 741–759. [CrossRef]
61. Ansdell, K.M.; Lucas, S.B.; Connors, K.; Stern, R.A. Kisseynew metasedimentary gneiss belt, Trans-Hudson orogen (Canada): Back-arc origin and collisional inversion. *Geology* **1995**, *23*, 1039–1043. [CrossRef]
62. Ansdell, K.M.; Kyser, T.K. Plutonism, deformation, and metamorphism in the Proterozoic Flin Flon greenstone belt, Canada: Limits on timing provided by the single-zircon Pb-evaporation technique. *Geology* **1991**, *19*, 518–521. [CrossRef]
63. Ashton, K.E.; Heaman, L.M.; Lewry, J.F.; Hartlaub, R.P.; Shi, R. Age and origin of the Jan Lake Complex: A glimpse at the buried Archean craton of the Trans-Hudson Orogen. *Can. J. Earth Sci.* **1999**, *36*, 185–208. [CrossRef]
64. Bickford, M.E.; Hamilton, M.A.; Wortman, G.L.; Hill, B.M. Archean rocks in the southern Rottenstone Domain: Significance for the evolution of the Trans-Hudson Orogen. *Can. J. Earth Sci.* **2001**, *38*, 1017–1025. [CrossRef]
65. Chiarenzelli, J.; Aspler, L.; Villeneuve, M.; Lewry, J. Early proterozoic evolution of the saskatchewan craton and its allochthonous coyer, trans-hudson Orogen. *J. Geol.* **1998**, *106*, 247–267. [CrossRef]
66. Collerson, K.D.; Lewry, J.F.; Bickford, M.E.; Van Schmus, W.R. Crustal evolution of the buried Precambrian of southern Saskatchewan: Implications for diamond exploration. *Saskatchewan Geol. Soc. Spec. Publ.* **1990**, *10*, 150–165.

67. Gandhi, S.S.; Mortensen, J.K.; Prasad, N.; van Breemen, O. Magmatic evolution of the Southern Great Bear continental arc, Northwestern Canadian Shield: Geochronological constraints. *Can. J. Earth Sci.* **2001**, *38*, 767–785. [CrossRef]
68. Davis, W.J.; Kjarsgaard, B.A. A Rb-Sr phlogopite-whole rock isochron age for olivine minette from the Milk River area, southern Alberta. *Geol. Surv. Can.* **1994**, *1994-F*, 11–14. [CrossRef]
69. Kjarsgaard, B.A. Potassic magmatism in the Milk River area, southern Alberta: Petrology and economic potential. *Geol. Surv. Can.* **1994**, *1994*, 59–68.
70. Paces, J.B.; Miller, J.D. Precise U-Pb ages of Duluth Complex and related mafic intrusions, northeastern Minnesota: Geochronological insights to physical, petrogenetic, paleomagnetic, and tectonomagmatic processes associated with the 1.1 Ga Midcontinent Rift System. *J. Geophys. Res.* **1993**, *98*, 13997. [CrossRef]
71. Black, L.P.; Kamo, S.L.; Williams, I.S.; Mundil, R.; Davis, D.W.; Korsch, R.J.; Foudoulis, C. The application of SHRIMP to Phanerozoic geochronology; a critical appraisal of four zircon standards. *Chem. Geol.* **2003**. [CrossRef]
72. Mattinson, J.M. Analysis of the relative decay constants of235U and238U by multi-step CA-TIMS measurements of closed-system natural zircon samples. *Chem. Geol.* **2010**, *275*, 186–198. [CrossRef]
73. Mueller, P.A.; Kamenov, G.D.; Heatherington, A.L.; Richards, J. Crustal Evolution in the Southern Appalachian Orogen: Evidence from Hf Isotopes in Detrital Zircons. *J. Geol.* **2008**, *116*, 414–422. [CrossRef]
74. Ludwig, K.R. *User's Manual for Isoplot 3.00, a Geochronological Toolkit for Microsoft Excel.*; Berkeley Geochronology Center Special Publication No. 4; Berkeley Geochronological Center: Berkeley, CA, USA, 2003.
75. Ludwig, K.R. *User 's Manual for Isoplot 3.70*; Berkeley Geochronological Center: Berkeley, CA, USA, 2008.
76. Fisher, C.M.; Vervoort, J.D.; Hanchar, J.M. Guidelines for reporting zircon Hf isotopic data by LA-MC-ICPMS and potential pitfalls in the interpretation of these data. *Chem. Geol.* **2014**, *363*, 125–133. [CrossRef]
77. Vervoort, J.D.; Patehett, P.J.; Söderlund, U.; Baker, M. Isotopie composition of Yb and the determination of Lu concentrations and Lu/Hf ratios by isotope dilution using MC-ICPMS. *Geochem. Geophys. Geosyst.* **2004**, *5*, 1–15. [CrossRef]
78. Woodhead, J.D.; Hergt, J.M. A Preliminary Appraisal of Seven Natural Zircon Reference Materials for In Situ Hf Isotope Determination. *Geostand. Geoanal. Res.* **2005**, *29*, 183–195. [CrossRef]
79. Söderlund, U.; Patchett, P.J.; Vervoort, J.D.; Isachsen, C.E. The 176Lu decay constant determined by Lu-Hf and U-Pb isotope systematics of Precambrian mafic intrusions. *Earth Planet. Sci. Lett.* **2004**, *219*, 311–324. [CrossRef]
80. Scherer, E.E.; Munker, C.; Mezger, K. Calibration of the Lutetium-Hafnium Clock. *Science* **2001**, *293*, 683–688. [CrossRef] [PubMed]
81. Griffin, W.L.; Pearson, N.J.; Belousova, E.; Jackson, S.E.; Van Achterbergh, E.; O'Reilly, S.Y.; Shee, S.R. The Hf isotope composition of cratonic mantle: LAM-MC-ICPMS analysis of zircon megacrysts in kimberlites. *Geochim. Cosmochim. Acta* **2000**, *64*, 133–147. [CrossRef]
82. Griffin, W.L.; Wang, X.; Jackson, S.E.; Pearson, N.J.; O'Reilly, S.Y.; Xu, X.; Zhou, X. Zircon chemistry and magma mixing, SE China: In-situ analysis of Hf isotopes, Tonglu and Pingtan igneous complexes. *Lithos* **2002**, *61*, 237–269. [CrossRef]
83. DePaolo, D.J.; Wasserburg, G.J. Nd isotopic variations and petrogenetic models. *Geophys. Res. Lett.* **1976**. [CrossRef]
84. Bouvier, A.; Vervoort, J.D.; Patchett, P.J. The Lu-Hf and Sm-Nd isotopic composition of CHUR: Constraints from unequilibrated chondrites and implications for the bulk composition of terrestrial planets. *Earth Planet. Sci. Lett.* **2008**, *273*, 48–57. [CrossRef]
85. Jones, R.E.; van Keken, P.E.; Hauri, E.H.; Tucker, J.M.; Vervoort, J.; Ballentine, C.J. Origins of the terrestrial Hf-Nd mantle array: Evidence from a combined geodynamical-geochemical approach. *Earth Planet. Sci. Lett.* **2019**. [CrossRef]
86. Sanfilippo, A.; Salters, V.; Tribuzio, R.; Zanetti, A. Role of ancient, ultra-depleted mantle in Mid-Ocean-Ridge magmatism. *Earth Planet. Sci. Lett.* **2019**, *511*, 89–98. [CrossRef]
87. Staffenberg, J.; Mueller, P.A.; Mogk, D.W.; Henry, D.J.; Wooden, J.L. Testing a model of 2.8 Ga arc genesis with trace elements. *Geol. Soc. Am. Abstr. Programs* **2011**, *43*, 435.

88. Weiss, R.A.; Vogl, J.J.; Mueller, P.A.; Foster, D.A.; Kamenov, G.D.; Wooden, J.L. Lu-Hf Analysis of Zircons in the Little Belt Mountains Suggest Paleoproterozoic Subduction in the Great Falls Tectonic Zone. In Proceedings of the American Geophysical Union (AGU) Fall 2009 Meeting, San Francisco, CA, USA, 13–18 December 2009; V43E-2321.
89. Joswiak, D.J. Composition and evolution of the lower crust, central Montana: Evidence from granulite xenoliths. Master's Thesis, University of Washington, Seattle, WA, USA, 1992.
90. Rudnick, R.L.; Gao, S. Composition of the Continental Crust. *Treatise Geochem.* **2003**, *3*, 1–64.
91. Frost, C.D.; Burwash, R.A. Nd evidence for extensive Archean basement in the western Churchill province, Canada. *Can. J. Earth Sci.* **1986**, *23*, 1433–1437. [CrossRef]
92. Stevenson, R.K.; Patchett, P.J. Implications for the evolution of continental crust from Hf isotope systematics of Archean detrital zircons. *Geochim. Cosmochim. Acta* **1990**. [CrossRef]
93. Mogk, D.W.; Burger, H.R.; Mueller, P.A.; D'Arcy, K.; Heatherington, A.L.; Wooden, J.L.; Abeyta, R.L.; Martin, J.; Jacob, L.J. Geochemistry of quartzofeldspathic gneisses and metamorphic mafic rocks of the indian creek and pony-middle mountain Metamorphic suites, Tobacco root Mountains, Montana. In *Precambrian Geology of the Tobacco Root Mountains, Montana*; Geological Society of America: Boulder, CO, USA, 2004; Volume 377, ISBN 0813723779.
94. Krogh, T.E.; Kamo, S.L.; Hanley, T.B.; Hess, D.F.; Dahl, P.S.; Johnson, R.E. Geochronology and geochemistry of Precambrian gneisses, metabasites, and pegmatite from the Tobacco Root Mountains, northwestern Wyoming craton, Montana. *Can. J. Earth Sci.* **2011**, *48*, 161–185. [CrossRef]
95. Mueller, P.A.; Heatherington, A.L.; D'Arcy, K.A.; Wooden, J.L.; Nutman, A.P. Contrasts between Sm-Nd whole-rock and U-Pb zircon systematics in the Tobacco Root batholith, Montana: Implications for the determination of crustal age provinces. *Tectonophysics* **1996**, *265*, 169–179. [CrossRef]
96. Brewer, R.A.; Vervoort, J.D.; Lewis, R.S.; Gaschnig, R.M.; Hart, G. New constraints on the extent of Paleoproterozoic and Archean basement in the Northwest U.S. cordillera. In Proceedings of the American Geophysical Union (AGU) Fall 2008 Meeting, San Francisco, CA, USA, 15–19 December 2009; Volume 89, Abstract T23C-2066.
97. Jansen, A.C.; Vervoort, J.D.; Lewis, R.S. Precambrian basement rocks of the Clearwater metamorphic complex: A new piercing point along the western margin of Laurentia. *GSA Abstr. Programs* **2011**, *43*, 491.
98. Lewis, R.S.; Brewer, R.A.; Jansen, A.C.; Guevara, V.E.; Vervoort, J.D.; Baldwin, J.A. Below the Belt: A road log in the eastern Clearwater Complex, Idaho. *Northwest Geol.* **2011**, *40*, 143–158.
99. Vervoort, J.D.; Lewis, R.S.; Fisher, C.; Gaschnig, R.M.; Jansen, A.C.; Brewer, R. Neoarchean and Paleoproterozoic crystalline basement rocks of north-central Idaho: Constraints on the formation of western Laurentia. *Bull. Geol. Soc. Am.* **2015**, *128*, 94–109. [CrossRef]
100. Burrett, C.; Berry, R. Proterozoic Australia-Western United States (AUSWUS) fit between Laurentia and Australia. *Geology* **2000**, *28*, 103–106. [CrossRef]
101. Thorkelson, D.J.; Laughton, J.R. Paleoproterozoic closure of an Australia-Laurentia seaway revealed by megaclasts of an obducted volcanic arc in Yukon, Canada. *Gondwana Res.* **2016**, *33*, 115–133. [CrossRef]
102. Ross, G.M.; Eaton, D.W.; Boerner, D.E.; Miles, W. Tectonic entrapment and its role in the evolution of continental lithosphere: An example from the Precambrian of western Canada. *Tectonics* **2000**, *19*, 116–134. [CrossRef]
103. Karlstrom, K.E.; Harlan, S.S.; Williams, M.L.; McLelland, J.; Geissman, J.W.; Åhäll, K.I. Refining Rodinia: Geologic evidence for the Australia-Western U.S. Connection in the Proterozoic. *GSA Today* **1999**, *9*, 2–7. [CrossRef]
104. Thorkelson, D.J.; Mortensen, J.K.; Creaser, R.A.; Davidson, G.J.; Abbott, J.G. Early proterozoic magmatism in Yukon, Canada: Constraints on the evolution of Northwestern Laurentia. *Can. J. Earth Sci.* **2001**, *38*, 1479–1494. [CrossRef]
105. Medig, K.P.R.; Thorkelson, D.J.; Davis, W.J.; Rainbird, R.H.; Gibson, H.D.; Turner, E.C.; Marshall, D.D. Pinning northeastern Australia to northwestern Laurentia in the Mesoproterozoic. *Precambrian Res.* **2014**, *249*, 88–99. [CrossRef]
106. O'Neill, J.M.; Duncan, M.S.; Zartman, R.E. An Early Proterozoic gneiss dome in the Highland Mountains, southwestern Montana. *Mont. Bur. Mines Geol. Spec. Publ.* **1988**, *96*, 81–88.

107. Mueller, P.A.; Wooden, J.L.; Mogk, D.W.; Nutman, A.P.; Williams, I.S. Extended history of a 3.5 Ga trondhjemitic gneiss, Wyoming Province, USA: Evidence from U-Pb systematics in zircon. *Precambrian Res.* **1996**, *78*, 41–52. [CrossRef]
108. Krogh, T.E.; Kamo, S.L.; Hess, D.F. Wyoming province 3300+ Ma gneiss with 2400 Ma metamorphism, northwestern Tobacco Root Mountains, Madison County, Montana. *Geol. Soc. Am. Abstr. Programs* **1997**, *29*, A408.
109. Whitmeyer, S.J.; Karlstrom, K.E. Tectonic model for the Proterozoic growth of North America. *Geosphere* **2007**, *3*, 220–259. [CrossRef]